iScience

CellPress
OPEN ACCESS

Article

Multiple omics reveal link between the microbiota-gut-brain axis and intracranial aneurysm rupture

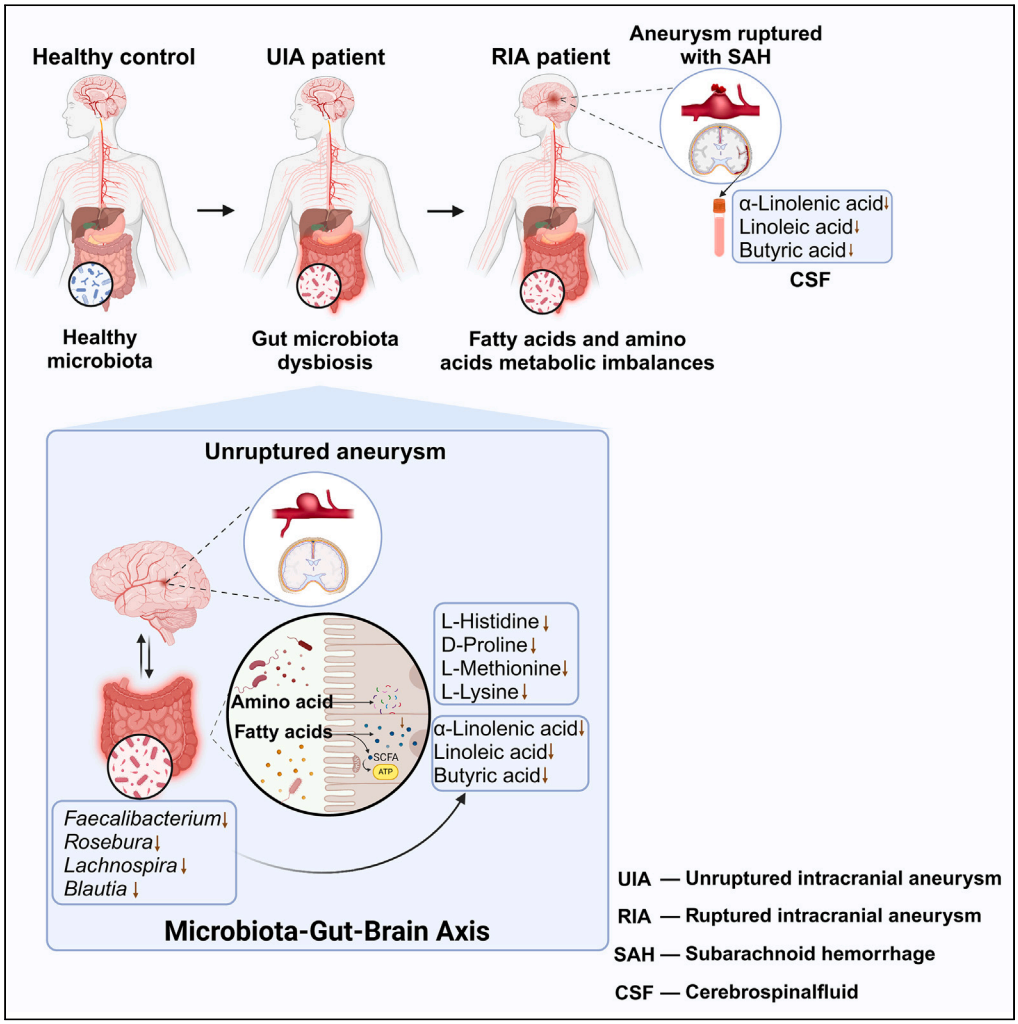

Hongyu Xu, Qiangqiang Zhou, Ziyue Xu, ..., Wei Wei, Zhengwei Li, Xiang Li

wei.wei@whu.edu.cn (W.W.)
lizhengwei1006@163.com (Z.L.)
li.xiang@whu.edu.cn (X.L.)

Highlights

IA patients exhibit gut microbiota dysbiosis compared to healthy family controls

Gut microbiota in RIA patients reveals dysbiosis of SCFAs and amino acids

Dysregulated gut-brain axis is closely linked to rupture events in IA

Gut microbiota of IA located at high-rupture-risk locations display unique profiles

Xu et al., iScience 27, 111184
November 15, 2024
https://doi.org/10.1016/j.isci.2024.111184

iScience

CellPress
OPEN ACCESS

Article

Multiple omics reveal link between the microbiota-gut-brain axis and intracranial aneurysm rupture

Hongyu Xu,[1,2] Qiangqiang Zhou,[1,2] Ziyue Xu,[1,2] Shengrong Long,[1,2] Gaomeng Luo,[1,2] Jincao Chen,[1,2,3] Wei Wei,[1,2,*] Zhengwei Li,[2,3,*] and Xiang Li[1,2,4,5,6,7,*]

SUMMARY

Intracranial aneurysms (IAs) are benign cerebrovascular maladies characterized by wall dilatation in the intracranial arteries. Nevertheless, spontaneous aneurysmal rupture can cause a life-threatening spontaneous subarachnoid hemorrhage (SAH). Emerging evidence indicates potential associations between gut dysbiosis and IAs pathogenesis, though the relationship with IA rupture remains unclear. This research analyzed 124 fecal samples for microbiomics and 160 for metabolomics, with the discovery and validation sets established for cross-validation. We identified differential gut microbiota and metabolites associated with ruptured intracranial aneurysms (RIAs) and developed a superior risk assessment model. Subsequent integrative analyses and validation revealed a significant link between disrupted unsaturated fatty acid and essential amino acid metabolic pathways and IA rupture, driven by alterations in gut microbiota. This study underscores the potential association between the gut-brain axis and IA rupture, while also highlighting gut microbiota dysbiosis as a potential risk factor for IA rupture and providing biomarkers for assessment.

INTRODUCTION

Intracranial aneurysms (IAs) are benign lesions of the cerebral blood vessels characterized by limited, pathological dilatation of the walls in the cerebral arteries.[1] Generally, aneurysms are divided into unruptured intracranial aneurysms (UIAs) and ruptured intracranial aneurysms (RIAs). As a predominant etiological factor in subarachnoid hemorrhage (SAH), RIAs are characterized by extremely high mortality rates and profound legacy of neurological deficits.[2] A follow-up study conducted in a Chinese population has revealed that patients with SAH exhibit a 28-day mortality rate of 19%.[3] Early detection of UIAs, along with accurate assessment of their rupture risk, is crucial in minimizing the occurrence of rupture events. Currently, the traditional rupture prediction model, the PHASES and ELAPSS score, fails to be effectively applied due to issues based on data from specific proactive cohort studies as well as research methodology.[4,5] To construct a comprehensive aneurysm rupture risk assessment system, it is imperative to explore perspectives on biological markers in combination with clinical characteristics for comprehensive assessment.

The microbiota-gut-brain axis (MGBA) concept has emerged, revealing fresh perspectives regarding the occurrence of neurological diseases and strategies for therapy.[6,7] The MGBA comprises a complex network of interactions among the gut microbiome, the nervous system, and the immune system.[8] It constitutes a bidirectional neurohumoral communication system, enabling the complex interplay between the brain and the gut microbiome. Through the hypothalamic-pituitary-adrenal (HPA) axis, the brain regulates the homeostasis of the gut microbiome, ensuring efficient metabolism and absorption of substances.[9] Conversely, neuroactive molecules and metabolites synthesized by the gut microbiome can traverse the blood-brain barrier (BBB), exerting biological function on the nervous system. Consequently, dysregulation of the gut microbiome can contribute to the occurrence of numerous neurological disorders including multiple sclerosis, Parkinson's disease, ischemic stroke, etc.[10–12] Recent studies have demonstrated that the gut microbiome dysbiosis-induced amino acid and fatty acid (FA) metabolism is involved in neurological disorders pathophysiological processes.[13,14] Short-chain fatty acids (SCFAs) have been identified to modulate protein and gene expression in the HPA axis, thereby attenuating the involvement of HPA axis responses in severe psychiatric disorders.[15] Concurrently, certain amino acids, including tryptophan and branched-chain amino acids, have emerged

[1]Brain Research Center, Zhongnan Hospital of Wuhan University, Wuhan University, Wuhan 430071, China
[2]Department of Neurosurgery, Zhongnan Hospital of Wuhan University, Wuhan University, Wuhan 430071, China
[3]Hubei Provincial Clinical Research Center for Cerebrovascular Severe Disease, Zhongnan Hospital of Wuhan University, Wuhan 430071, China
[4]Frontier Science Center for Immunology and Metabolism, Wuhan University, Wuhan 430072, China
[5]Medical Research Institute, Wuhan University, Wuhan 430072, China
[6]Sino-Italian Ascula Brain Science Joint Laboratory, Wuhan University, Wuhan 430071, China
[7]Lead contact
*Correspondence: wei.wei@whu.edu.cn (W.W.), lizhengwei1006@163.com (Z.L.), li.xiang@whu.edu.cn (X.L.)
https://doi.org/10.1016/j.isci.2024.111184

as pivotal players in the MGBA and present the potential for therapeutic targeting through endocrine regulation.[16] This is achieved by influencing the synthesis of key hormones, such as melatonin and glucocorticoids. Recently, clinical sequencing has confirmed the presence of gut dysbiosis in patients with UIAs.[17] However, there is no direct evidence linking the RIAs to dysbiosis of gut microbiome and metabolites. Urgent research is needed to identify biomarkers of relevant rupture risk-associated gut microbiome and metabolites that will allow early assessment of aneurysm rupture risk.

The advancement of third-generation sequencing has facilitated the application of multi-omics analyses combining microbiomics and metabolomics to better reveal microbial interactions with metabolites.[18] The influence of gut microbiome on the biochemical and physiological functions within the host can be explored while understanding the diversity of microbes. In this study, we employed multi-omics analysis to identify the differences in fecal metabolites and dysbiosis in the gut microbiome of a group of patients with UIA and RIA and family controls. The study revealed that disruption in lipid and amino acid metabolism, attributed to disturbances in the gut microbiota, is evident in the stool of RIA patients. Screening for divergent core gut microbiome and metabolites, we identified key gut microbiome and metabolites associated with aneurysm rupture while constructing excellent diagnostic models to differentiate whether an aneurysm is ruptured or not. In addition, we further revealed alterations in the gut microbiome of patients with IAs at high-risk rupture locations, incorporating the clinical characteristics. Finally, we verified changes in α-linolenic acid, butyric acid, and linoleic acid levels through peripheral blood (PB) and cerebrospinal fluid (CSF) samples. This research suggests the potential association between gut microbial dysbiosis and the occurrence and development of IAs by revealing abnormalities in the gut microbiome and its metabolites, thus providing possible risk assessment biomarkers for UIAs.

RESULTS

Study overview

The study overview is presented in Figure 1. To explore the gut flora and metabolites from UIA or RIA patients, in total 124 fecal samples for 16s rRNA microbiomics sequencing and 160 fecal samples for untargeted metabolomics analysis were collected. Tables 1 and 2 list the clinical characteristics of all participants. PB and intraoperative CSF samples from thirty patients were recollected to measure the concentrations of butyric acid, α-linolenic acid, and linoleic acid by ELISA. A total of 2,876,103 circular consensus sequencing (CCS) reads were generated after barcode identification, and an average of 16,393 valid CCS reads per sample were generated following filtering for internal reference sequences (70 samples from 27 UIA patients, 18 controls and 25 RIA patients in the exploratory cohort; 54 samples from 25 UIA patients, 19 controls, and 10 RIA patients in the validation cohort). Read counts were clustered at 97.0% similarity using the USEARCH software to obtain the operational taxonomic unit (OTU) counts for each sample for subsequent microbiomics analyses.[19] After excluding samples failing quality control, 66 matched fecal samples from the microbiome discovery set were reserved for untargeted metabolomics analysis. In parallel, stool samples from 94 patients were acquired as a validation set for metabolomics data analysis. For subsequent metabolomics analyses, the screening of differential metabolites involved a composite assessment incorporating multiplicity differences, *p* values, and VIP values derived from the orthogonal partial least squares-discriminant analysis (OPLS-DA) model.

Dysfunctional species diversity of the gut microbiome in patients with IA

In the exploratory cohort, a total of 773 OTUs were annotated from 2,876,103 CCS reads obtained by 16s rRNA sequencing in 70 stool samples (Figure 2A). Venn diagrams represent the differential OTUs among the normal control (NC), UIA, and RIA groups, with 28, 29, and 100 characteristic OTUs detected, respectively. (Figure 2B). At the phylum level, *Firmicutes*, *Proteobacteria*, and *Bacteroidetes* are the most predominant phyla in the stools from family control and patients with IAs, comprising 95.8%, 94.8%, and 91.3% of the stools in NC, UIA and RIA patients, respectively (Figure 2C). In the IA patient group, particularly in the RIA group, the abundance of *Firmicutes* was significantly decreased compared to both the family control and UIA groups ($p < 0.05$). Conversely, *Proteobacteria* abundance was significantly increased in RIA compared to the family control ($p < 0.05$). The abundance of *Bacteroidota* tended to increase in RIA compared to UIA and family control, though the difference was not statistically significant (Figure 2D). This indicates that the gut microbiota in the UIA and RIA groups may differ from that in the NC group. The Shannon index curves for the NC, UIA, and RIA groups were flattened, indicating that the sample sizes were adequate and covered the majority of the microbial species information (Figure 2E). To confirm the altered gut microbial community structure in patients with IAs, we performed an alpha diversity analysis. The alpha diversity of the gut flora in RIAs was significantly lower, as indicated by the Shannon and Simpson indices, compared to the other groups. (Figures 2F–2I, $p < 0.05$). No significant differences were observed for the community richness indices (Chao and abundance-based coverage estimator [ACE] metric) and coverage index, but a tendency for ACE and Chao index to decrease was noted in the RIA group compared to the UIA and healthy control groups (Figure S1A). In addition, the microbial composition was analyzed by assessing beta diversity with non-metric multi-dimensional scaling (NMDS) and analysis of similarities (ANOSIM). Significant discrepancies were found between UIA, RIA, and normal control by NMDS analysis based on Bray-Curtis distances (Figure 2J, Stress < 0.2). ANOSIM analysis showed meaningful distinctions between the UIA, RIA, and normal control groups (Figure 2I, $R^2 = 0.132$, $p < 0.01$).

Identification and functional analysis of gut microbiota associated with RIAs

To elaborate on the identification of gut microbiota associated with the risk of IA rupture, we analyzed the comparative genus-level flora in the UIA, RIA, and normal control groups using the Kruskal-Wallis rank-sum test. In the exploratory cohort, a total of 61 differential

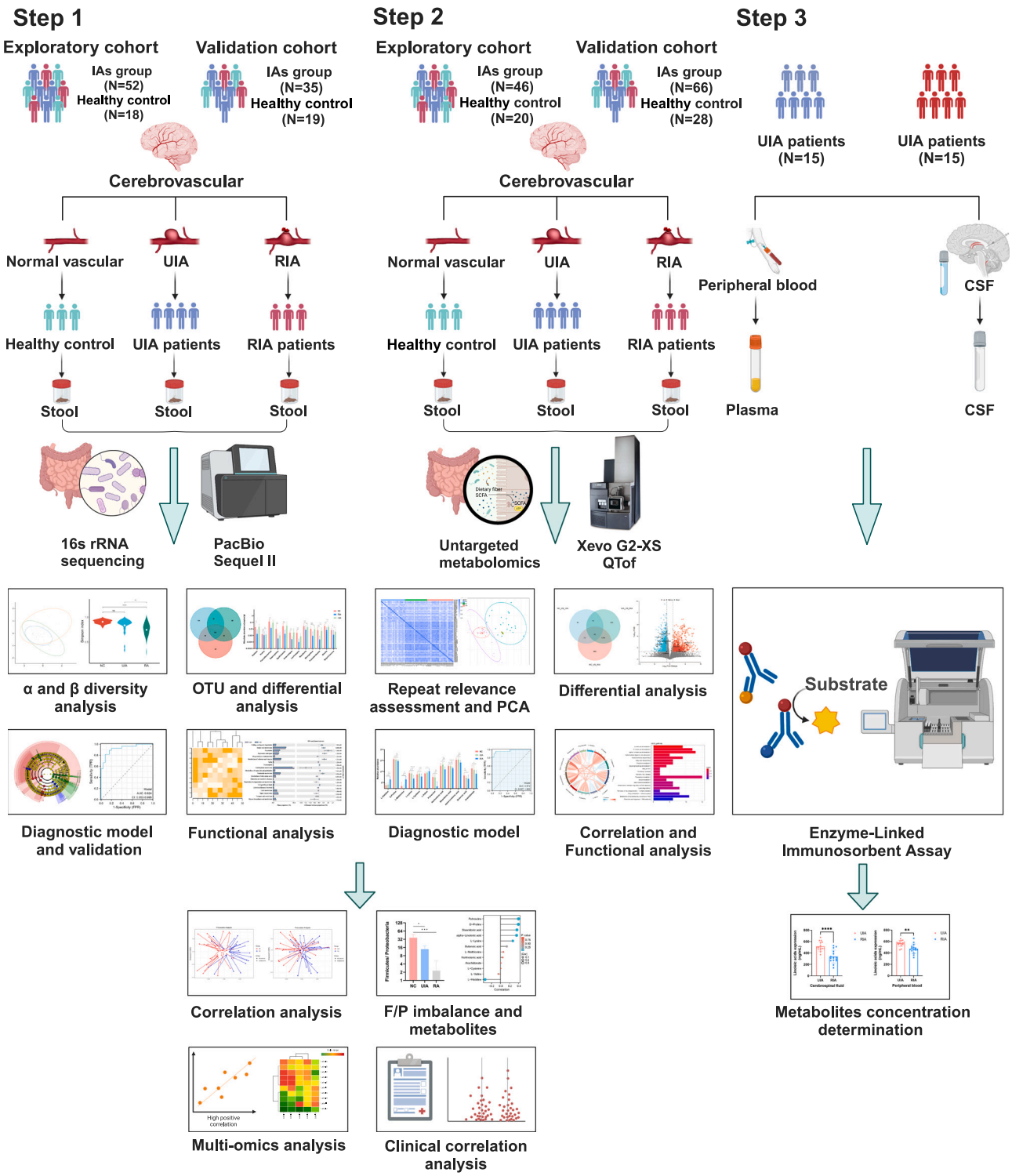

Figure 1. The flowchart of this study

16S rDNA sequencing and metabolomics analysis were performed on fecal samples from patients with IAs and healthy controls to identify potential factors associated with the risk of IAs formation and rupture.

Table 1. The basic clinical characteristics of intracranial aneurysms cases and healthy controls in microbiomics

	Exploratory cohort				Validation cohort			
Characteristics	NC	UIA	RIA	*p* value	NC	UIA	RIA	*p* value
n	18	27	25	–	19	25	10	–
Sex, n (%)				0.948				0.174
Male	8 (11.4%)	13 (18.6%)	11 (15.7%)	–	10 (18.5%)	8 (14.8%)	2 (3.7%)	–
Female	10 (14.3%)	14 (20%)	14 (20%)	–	9 (16.7%)	17 (31.5%)	8 (14.8%)	–
Age, n	55.1 ± 5.4	59.7 ± 7.8	57.6 ± 12.1	0.075	55.7 ± 8.12	57.6 ± 7.04	62.3 ± 9.7	0.121
Hypertension, n (%)				<0.001				<0.001
No	18 (25.7%)	12 (17.1%)	8 (11.4%)	–	19 (35.2%)	12 (22.2%)	5 (9.3%)	–
Yes	0 (0%)	15 (21.4%)	17 (24.3%)	–	0 (0%)	13 (24.1%)	5 (9.3%)	–
Diabetes, n (%)				0.056				0.171
No	18 (25.7%)	22 (31.4%)	24 (34.3%)	–	19 (35.2%)	22 (40.7%)	8 (14.8%)	–
Yes	0 (0%)	5 (7.1%)	1 (1.4%)	–	0 (0%)	3 (5.6%)	2 (3.7%)	–
CKD, n (%)				1				0.458
No	18 (25.7%)	26 (37.1%)	24 (34.3%)	–	19 (35.2%)	24 (44.4%)	9 (16.7%)	–
Yes	0 (0%)	1 (1.4%)	1 (1.4%)	–	0 (0%)	1 (1.9%)	1 (1.9%)	–
Smoking, n (%)				0.062				0.93
No	13 (18.6%)	21 (30%)	12 (17.1%)	–	16 (29.6%)	20 (37%)	8 (14.8%)	–
Yes	5 (7.1%)	6 (8.6%)	13 (18.6%)	–	3 (5.6%)	5 (9.3%)	2 (3.7%)	–
Drinking alcohol, n (%)				0.066				0.154
No	13 (18.6%)	23 (32.9%)	14 (20%)	–	16 (29.6%)	16 (29.6%)	9 (16.7%)	–
Yes	5 (7.1%)	4 (5.7%)	11 (15.7%)	–	3 (5.6%)	9 (16.7%)	1 (1.9%)	–
Aneurysm								
Size, n (mm)	–	5.67 ± 4.72	8.03 ± 4.43	–	–	6.90 ± 5.50	6.29 ± 3.07	–
Height-width ratio (HWR)	–	1.06 ± 0.95	1.99 ± 0.95	–	–	1.23 ± 0.43	1.31 ± 0.31	–
Location, n (%)				1				0.597
ICA	0 (0%)	17 (32.7%)	15 (28.8%)	–	0 (0%)	18 (51.4%)	5 (14.3%)	–
MCA	0 (0%)	2 (3.8%)	5 (9.6%)	–	0 (0%)	3 (8.6%)	3 (8.6%)	–
VA	0 (0%)	3 (5.8%)	2 (3.8%)	–	0 (0%)	2 (5.7%)	1 (2.9%)	–
Other arteries	0 (0%)	5 (9.6%)	3 (5.8%)	–	0 (0%)	2 (5.7%)	1 (2.9%)	–
Arterial bifurcation, n (%)				1				0.711
No	0 (0%)	14 (26.9%)	12 (23.1%)	–	0 (0%)	13 (37.1%)	4 (11.4%)	–
Yes	0 (0%)	13 (25.0%)	13 (25.0%)	–	0 (0%)	12 (34.3%)	6 (17.1%)	–
Multiple aneurysms, n (%)				0.79				0.381
No	0 (0%)	22 (42.3%)	22 (42.3%)	–	0 (0%)	21 (60.0%)	7 (20.0%)	–
Yes	0 (0%)	5 (9.6%)	3 (5.8%)	–	0 (0%)	4 (11.4%)	3 (8.6%)	–

floras were screened at the genus level and selected for demonstration and further analyses for which higher abundance and indicated critical biological roles were available (Figure 3A). *Faecalibacterium*, *Roseburia*, *Lachnospira*, and *Blautia*, the core gut bacteria, were significantly dysregulated in intracranial ruptured aneurysms. Together with *Butyricicoccus* and *Agathobacter*, they serve as the main producers of butyric acid and acetic acid.[20–22] Dysregulation of these gut microbiomes leads to disturbances in the metabolism of SCFAs and reduces the anti-inflammatory effect of the microbiome. Among the 61 divergently enriched species identified in the discovery set, 20 species (32.78%) were also prominently enriched in the ruptured aneurysm samples from the validation set (Figure S1B). Due to the essential influence of microbial interactions on the homeostasis and physiological functions within the host gastrointestinal flora, correlations were performed to analyze the differential flora.[23] Correlation analysis revealed a robust covariation of *Butyricicoccus* expression with *Faecalibacterium*, *Roseburia*, *Monoglobus*, and *Blautia*. Given their characteristic production of acetic and butyric acids, this observation suggests that these microorganisms may collectively contribute to the SCFA metabolism within the gut microbiota, thereby exerting a significant influence on the homeostatic regulation of the host's intestinal flora. *Lachnospira*, a fundamental flora specializing in carbohydrate metabolism, exhibited a close association with *Anaerostipes*, *Roseburia*, and *Blautia*.[24] Besides, its

Table 2. The basic clinical characteristics of intracranial aneurysms cases and healthy controls in metabolomics

	Exploratory cohort				Validation cohort			
Characteristics	NC	UIA	RIA	*p* value	NC	UIA	RIA	*p* value
n	20	24	22	–	28	40	26	–
Sex, n (%)				0.932				0.707
Male	9 (13.6%)	12 (18.2%)	10 (15.2%)	–	14 (14.9%)	16 (17%)	11 (11.7%)	–
Female	11 (16.7%)	12 (18.2%)	12 (18.2%)	–	14 (14.9%)	24 (25.5%)	15 (16%)	–
Age, n	55.1 ± 5.6	60.1 ± 8.2	57.6 ± 11.5	0.068	55.3 ± 11.7	57.4 ± 11.5	60.6 ± 9.9	0.229
Hypertension, n (%)				<0.001				<0.001
No	20 (30.3%)	11 (16.7%)	7 (10.6%)	–	28 (29.8%)	13 (13.8%)	5 (5.3%)	–
Yes	0 (0%)	13 (19.7%)	15 (22.7%)	–	0 (0%)	27 (28.7%)	21 (22.3%)	–
Diabetes, n (%)				0.093				0.239
No	20 (30.3%)	20 (30.3%)	21 (31.8%)	–	28 (29.8%)	36 (38.3%)	24 (25.5%)	–
Yes	0 (0%)	4 (6.1%)	1 (1.5%)	–	0 (0%)	4 (4.3%)	2 (2.1%)	–
CKD, n (%)				1				0.744
No	20 (30.3%)	23 (34.8%)	21 (31.8%)	–	28 (29.8%)	39 (41.5%)	25 (26.6%)	–
Yes	0 (0%)	1 (1.5%)	1 (1.5%)	–	0 (0%)	1 (1.1%)	1 (1.1%)	–
Smoking, n (%)				0.049				0.102
No	14 (21.2%)	19 (28.8%)	10 (15.2%)	–	21 (22.3%)	20 (21.3%)	14 (14.9%)	–
Yes	6 (9.1%)	5 (7.6%)	12 (18.2%)	–	7 (7.4%)	20 (21.3%)	12 (12.8%)	–
Drinking alcohol, n (%)				0.089				0.392
No	15 (22.7%)	20 (30.3%)	12 (18.2%)	–	10 (10.6%)	21 (22.3%)	12 (12.8%)	–
Yes	5 (7.6%)	4 (6.1%)	10 (15.2%)	–	18 (19.1%)	19 (20.2%)	14 (14.9%)	–
Aneurysm								
Size, n (mm)	–	4.8 ± 2.7	7.2 ± 2.6	–	–	6.6 ± 6.2	7.7 ± 3.3	–
Height-width ratio (HWR)	–	0.87 ± 0.53	1.87 ± 0.66	–	–	1.21 ± 0.33	1.28 ± 0.48	–
Location, n (%)				1				0.820
ICA	0 (0%)	16 (34.8%)	14 (30.4%)	–	0 (0%)	22 (33.3%)	13 (19.7%)	–
MCA	0 (0%)	2 (4.3%)	4 (8.7%)	–	0 (0%)	9 (13.6%)	7 (10.6%)	–
VA	0 (0%)	3 (6.5%)	2 (4.3%)	–	0 (0%)	5 (7.6%)	2 (3.0%)	–
Other arteries	0 (0%)	3 (6.5%)	2 (4.3%)	–	0 (0%)	4 (6.1%)	4 (6.1%)	–
Arterial bifurcation, n (%)				1				0.614
No	–	13 (28.3%)	11 (23.9%)	–	–	21 (31.8%)	12 (18.2%)	–
Yes	–	11 (23.9%)	11 (23.9%)	–	–	19 (28.8%)	14 (21.2%)	–
Multiple aneurysms, n (%)				1				1
No	–	20 (43.5%)	19 (41.3%)	–	–	36 (54.5%)	23 (34.8%)	–
Yes	–	4 (8.7%)	3 (6.5%)	–	–	4 (6.1%)	3 (4.5%)	–

expression was notably downregulated in the RIA groups, implicating that disturbances in carbohydrate metabolism could be intricately linked to aneurysm rupture (Figure 3B). Afterward, we searched for differential critical species associated with the aneurysm rupture at the genus level by linear discriminant analysis effect size (LEfSe) analysis as well as random forest analysis as biomarkers for the aneurysm rupture risk prediction model (Figures 3C and 3D). Subsequently, Lasso regression analysis was conducted to identify suitable diagnostic markers of the gut microbiome, with the top 25 species being evaluated based on the mean decrease Gini values obtained from random forest analysis. In the discovery set, we employed the nine screened gut microbiomes (*Bacillus*, *TM7x*, *Fusicatenibacter*, *Rikenellaceae_RC9_gut_group*, *Butyricicoccus*, *Blautia*, *Granulicatella*, *Rothia*, and *Dorea*) to construct receiver operating characteristic (ROC) curves for distinguishing unruptured aneurysms from ruptured aneurysms, excluding *Lachnospiraceae_UCG_004* from the model due to the risk of overfitting. The area under the curve (AUC) was as high as 0.970, with confidence intervals (CI) ranging from 0.933 to 1.000. Consistent with the outcome in the discovery set, the validation set showed an AUC of 0.888 and a CI of 0.771–1.000 (Figure 3E). BugBase was subsequently applied to predict the functional phenotype in the gut flora. Gram-negative, facultatively anaerobic,

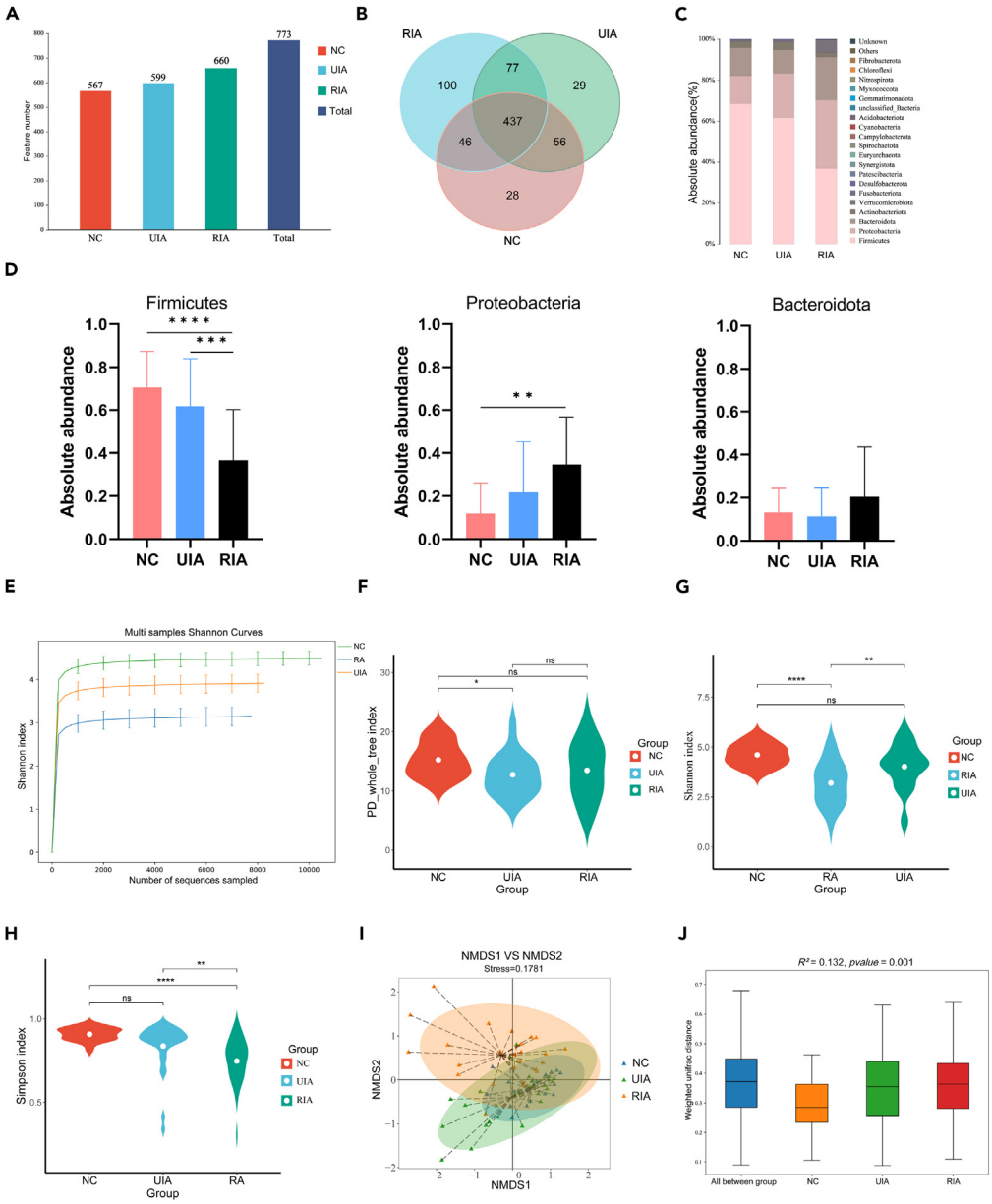

Figure 2. Dysbiosis of the gut microbiota in patients with intracranial aneurysms

(A) Distribution of the number of features in each group.

(B) Venn diagram depicting the quantity of both shared and distinct OTUs among various groups.

(C) Species composition of the gut microbiota in groups at the portal level.

(D) Species abundance of *Firmicutes*, *Proteobacteria*, and *Bacteroidetes* in family control, UIA, and RIA (one-way ANOVA, mean with SD). *p* value, $^{**}p < 0.01$; $^{***}p < 0.001$; $^{****}p < 0.001$.

(E) Shannon diversity index curve utilized to evaluate the sufficiency of sample size and sequencing depth.

(F–I) Alpha diversity index variance analysis and beta diversity analysis (Wilcoxon test, mean with SD). *p* value, $^{*}p < 0.05$; $^{**}p < 0.01$; $^{****}p < 0.001$.

(J) Permutational multivariate analysis of variance analysis to assess similarity between samples of different subgroups (permutation test, mean with SD). *p* value, $^{**}p < 0.01$.

potentially pathogenic, and stress-tolerant phenotypes were enormously increased in the RIAs (Figure 3F). Differential pathways in the RIA group compared to the UIA and normal control groups were afterward analyzed by PICRUSt2. Differential metabolic pathways in the RIA group included translation, amino acid metabolism, lipid metabolism, and carbohydrate metabolism (Figure 3G). Consistent with the results of the identified differential flora, the reduction of SCFAs caused by the dysbiosis of *Faecalibacterium*, *Roseburia*, *Lachnospira*, and *Blautia* in the RIA group could be an eminent risk factor for the occurrence of RIAs.

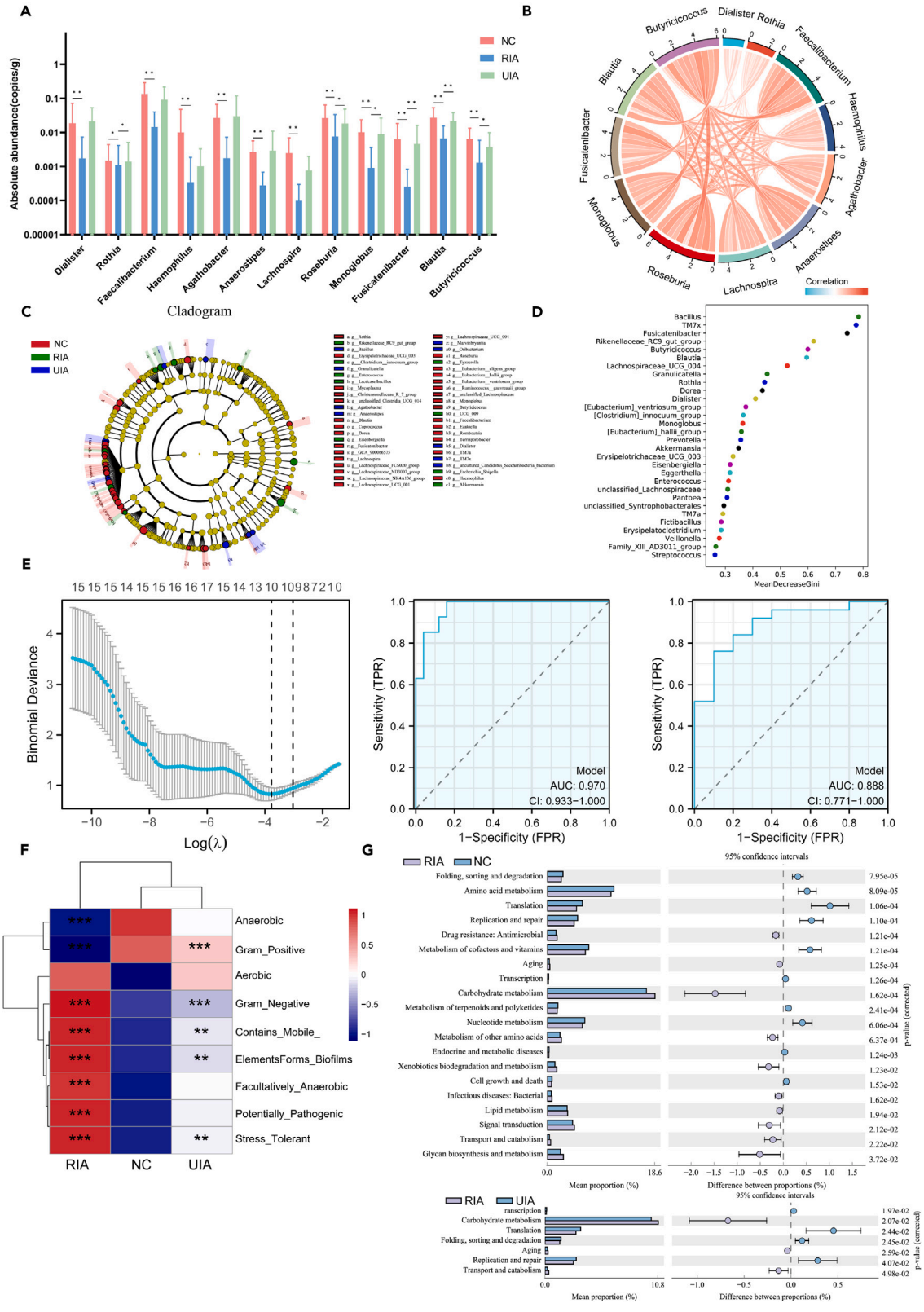
A
Absolute abundance(copies/g)
NC
RIA
UIA
Dialister
Rothia
Faecalibacterium
Haemophilus
Agathobacter
Anaerostipes
Lachnospira
Roseburia
Monoglobus
Fusicatenibacter
Blautia
Butyricicoccus
B
Correlation
C
Cladogram
D
MeanDecreaseGini
E
Binomial Deviance
Log(λ)
Sensitivity (TPR)
1−Specificity (FPR)
Model
AUC: 0.970
CI: 0.933−1.000
AUC: 0.888
CI: 0.771−1.000
F
Anaerobic
Gram_Positive
Aerobic
Gram_Negative
Contains_Mobile_
ElementsForms_Biofilms
Facultatively_Anaerobic
Potentially_Pathogenic
Stress_Tolerant
G
Mean proportion (%)
Difference between proportions (%)
95% confidence intervals
p-value (corrected)

Figure 3. Identification and functional analysis of gut microbiota associated with RIAs

(A) A histogram was constructed to illustrate the alterations in the species composition of gut microbiota at the genus level (Kruskal-Wallis rank-sum test, mean with SEM). *p* value, **p* < 0.05; ***p* < 0.01.

(B) Correlation chord plots effectively visualize the relationships between diverse bacterial populations.

(C and D) LEfSe and random forest analysis to identify biomarkers for the aneurysm rupture risk prediction model.

(E) Lasso algorithm for screening ROC correlation coefficients and ROC curves for differentiating unruptured from ruptured aneurysms.

(F and G) Functional and phenotypic prediction of gut microbiota using PICRUSt2 and BugBase (Fisher's exact test). *p* value, ***p* < 0.01; ****p* < 0.001.

Identification of differential metabolites in IA fecal samples

Given the apparent regulatory role of the gut flora on metabolites and the aforementioned findings, 66 matched stool samples from the microbiome discovery set were reserved for untargeted metabolomics analysis. At the same time, we collected 94 fecal samples as a validation set for metabolomic analysis. Repeat relevance assessment demonstrated great repeatability between samples within groups (Figure 4A). Principal-component analysis (PCA) and OPLS-DA showed differences in overall metabolites between the RIA group and UIA and normal groups (NC-RIA: R2Y = 0.996, Q2Y = 0.806; UIA-RIA: R2Y = 0.996, Q2Y = 0.774) (Figure 4B). The cross-validation demonstrated the reliability of the OPLS-DA models and predictions (Figure S1C). In the validation set samples, the results of PCA and repeat relevance assessment exhibited strong concordance with those obtained from the discovery set, indicating the reliability and reproducibility of our findings (Figure S1D). The volcano diagram illustrates the 1,974 and 1,762 differential metabolites identified in the RIA group compared to the UIA and normal control groups, respectively. Among them, 1,443 shared differential metabolites were identified in the RIA group compared to the other two groups (Figures 4C and 4D). Subsequently identified differentially enriched metabolites were utilized for Kyoto Encyclopedia of Genes and Genomes (KEGG) analysis. Surprisingly, amino acid metabolism, lipid metabolism, and carbohydrate metabolism were the main enriched pathways in the RIAs, which was highly consistent with the microbiomics results (Figure 4E). The validation set findings were highly concordant with the discovery set, confirming further that dysregulation of lipid metabolism and amino acid metabolism is heavily correlated with rupture of IAs (Figure S1E). Therefore, we selected the core metabolites of lipid metabolism, amino acid metabolism, and carbohydrate metabolism to be displayed and used in the combined multi-omics analyses (Figure 4F). Data from the validation set confirmed that some FAs were enriched with amino acids similarly to the discovery set, including linoleic acid, α-linolenic acid, and several essential amino acids (Figure S1F). Meanwhile, correlation analysis was applied to reveal the correlation network between FAs and amino acids (Figure 4G). Afterward, we constructed an ROC diagnostic model of the divergently enriched core metabolites for separating patients with RIA versus patients with UIA. The AUC was as high as 0.972, with CI ranging from 0.927 to 1.000). Consistent with the outcome in the discovery set, the validation set showed an AUC of 0.919 and a CI of 0.857–0.981 (Figure 4H).

Combined multi-omics analysis of the gut microbiome and its metabolites in IA patients

To investigate the combined function of gut microbiota and metabolites in the progression of IAs, we simultaneously analyzed metabolomics and microbiomics data along with clinical information of the patients. Procrustes analysis suggested that microbiomics abundance followed a highly pronounced trend with metabolomics expression (Figure 5A). The analysis initially focused on the alterations in *Firmicutes* and *Proteobacteria*, which are the two most abundant species in IA patients. Analysis showed that the *Firmicutes*/*Proteobacteria* (F/P) ratio was significantly lower in the IA group, especially in RIA (Figure 5B). This implies that abnormalities in F/P may be related to the occurrence of IA or even serve as a risk factor for aneurysm rupture. Furthermore, the Pearson analysis showed that putrescine, D-proline, α-linolenic acid, and stearidonic acid had positive correlation with F/P, while L-histidine was negatively correlated with F/P. We analyzed the 24 differentially enriched microbes and metabolites that were previously shown to reveal the regulatory role between flora and metabolites in IA patients (Figure 5C). Proline, a crucial amino acid essential for enhancing vascular elasticity and compliance, exhibits a positive association with dysbiosis in various species, notably *Butyricicoccus*, *Roseburia*, and *Monoglobus* ($R > 0.55$, $p < 0.05$). This observation implies that the downregulation of proline levels triggered by dysbiosis may serve as a contributory factor in the decreased elasticity and subsequent rupture of aneurysmal walls. Similarly, loss of α-linolenic acid as a cardio-protective factor is closely related to the disorders of various floras such as *Butyricicoccus* and *Faecalibacterium* ($R > 0.50$, $p < 0.05$). In addition, for IAs, age, sex, and especially maximum aneurysm diameter and aneurysm aspect ratio are strongly associated with the risk of rupture (Figure 5D).[25] Finally, we determined the concentrations of butyric acid, α-linolenic acid, and linoleic acid in PB and paired CSF samples from 15 patients with UIA and 15 patients with RIA. This suggests that the reduction of butyric acid, α-linolenic acid, and linoleic acid due to dysbiosis of the gut flora crosses the BBB via the MGBA and acts on the cerebral vessels, which are further involved in the process of IAs (Figure 5E).

Altered gut microbiome in patients with IAs is tightly linked to site of occurrence

For IAs, the location of occurrence is intimately linked to the rupture risk. In particular, aneurysms located in the posterior circulation, the internal carotid artery, and the middle cerebral artery bifurcation are more likely to rupture than other location.[26,27] Therefore, we classified 87 patients with IA into high- and low-rupture-risk groups according to the location of the aneurysm for microbiomics analysis. The Venn diagram illustrates common and distinct species identified between the two groups at the OTU level (Figure 6A). Analogous to the results in the RIA group, the species distribution displayed a downregulation of the abundance of *Firmicutes* in the high-risk group and a corresponding increase in the abundance of *Proteobacteria* (Figure 6B). Alpha diversity analysis reveals significantly lower diversity and abundance of gut microbiota in IAs located in posterior circulation, Acom, Pcom, and middle cerebral artery (MCA) aneurysms (Figure 6C). Partial least squares

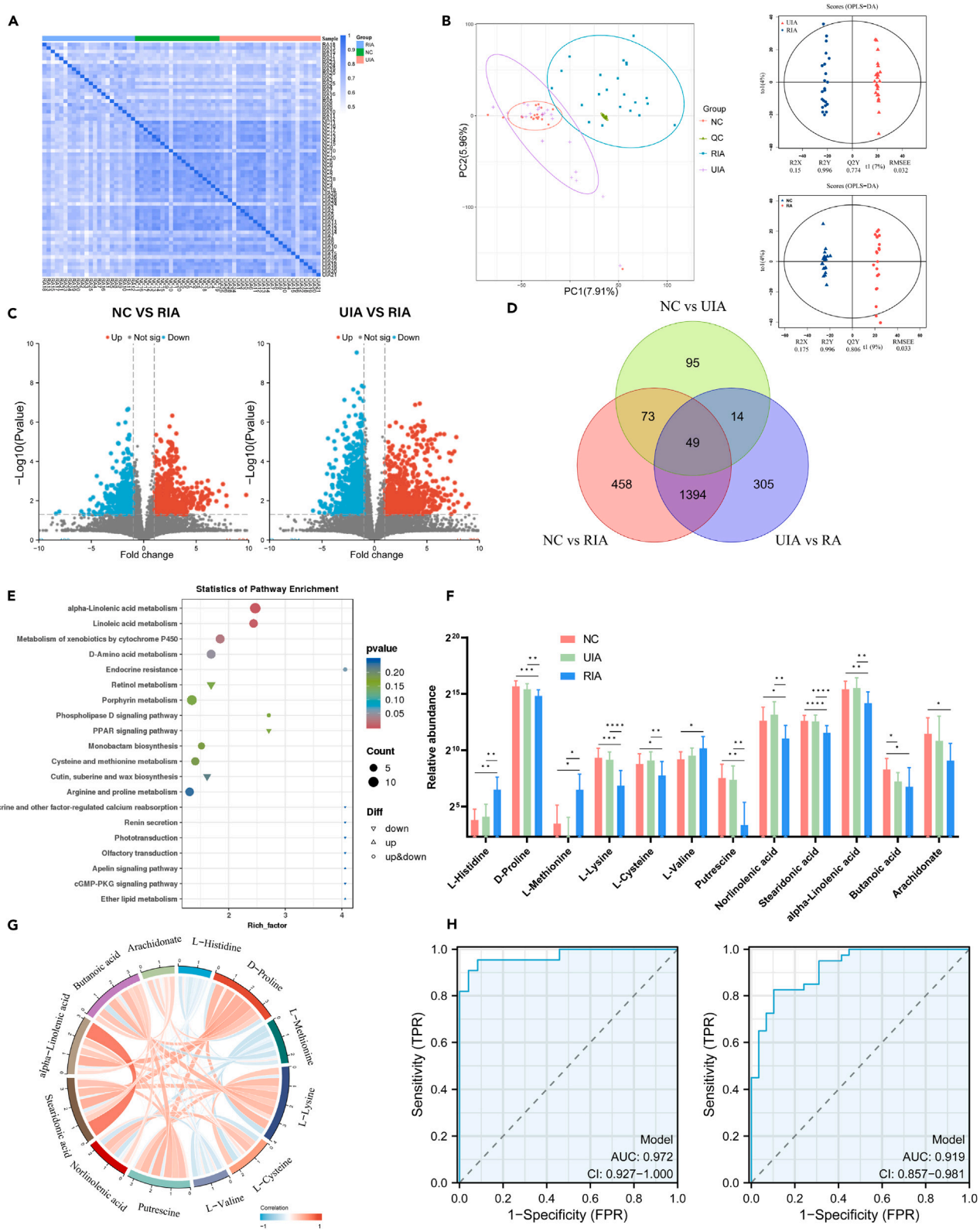
A
B
C
NC VS RIA
UIA VS RIA
Up
Not sig
Down
−Log10(Pvalue)
Fold change
D
NC vs UIA
95
73
14
49
458
1394
305
NC vs RIA
UIA vs RA
E
Statistics of Pathway Enrichment
alpha-Linolenic acid metabolism
Linoleic acid metabolism
Metabolism of xenobiotics by cytochrome P450
D-Amino acid metabolism
Endocrine resistance
Retinol metabolism
Porphyrin metabolism
Phospholipase D signaling pathway
PPAR signaling pathway
Monobactam biosynthesis
Cysteine and methionine metabolism
Cutin, suberine and wax biosynthesis
Arginine and proline metabolism
Endocrine and other factor-regulated calcium reabsorption
Renin secretion
Phototransduction
Olfactory transduction
Apelin signaling pathway
cGMP-PKG signaling pathway
Ether lipid metabolism
Rich_factor
pvalue
Count
Diff
down
up
up&down
F
NC
UIA
RIA
Relative abundance
L-Histidine
D-Proline
L-Methionine
L-Lysine
L-Cysteine
L-Valine
Putrescine
Norlinolenic acid
Stearidonic acid
alpha-Linolenic acid
Butanoic acid
Arachidonate
G
H
Sensitivity (TPR)
1−Specificity (FPR)
Model
AUC: 0.972
CI: 0.927−1.000
AUC: 0.919
CI: 0.857−0.981

Figure 4. Identification of differential metabolites in intracranial aneurysms

(A) Correlation coefficient matrix analysis between samples to assess biological replication between samples within groups.

(B) PCA and OPLS-DA score plots in IAs and control samples.

(C and D) Volcano and Wayne plots showing the quantity of differential metabolites identified.

(E) KEGG enrichment analysis for differential metabolism in discovery set.

(F) Plotting histograms to illustrate variation in the abundance of metabolites associated with amino acid and lipid metabolism (Kruskal-Wallis rank-sum test, mean with SEM). *p* value, **p* < 0.05; ***p* < 0.01; ****p* < 0.001; *****p* < 0.001.

(G) Correlation chord plots effectively visualize the relationships between diverse metabolites.

(H) ROC curves for differentiating unruptured from ruptured aneurysms.

discriminant analysis (PLS-DA) was able to discriminate well between the two groups (Figure 6D). We then proceeded to identify the divergent species (at the genus level) between the two groups by Metastats analysis and selected species for display based on higher abundance and critical biological roles (Figure 6E). *Roseburia*, *Agathobacter*, *Butyricicoccus*, *Rothia*, and *Blautia* were prominently dysbiosis species in posterior circulation, Acom, Pcom, and MCA aneurysms. These results further demonstrated the relevance of gut microbiota dysbiosis to RIA.

DISCUSSION

In recent years, the potential relationship between the gut microbiome and IAs has garnered increasing attention.[28–30] Nonetheless, the role of gut microbiota in IA rupture events has not been extensively studied, and comprehensive risk assessment models incorporating gut microbiota remain scarce. Distinguishing from prior research, our study conducted a multi-omics analysis encompassing both metabolomics and microbiome profiling, comparing fecal samples from patients with UIAs and RIAs, and healthy family controls. For microbiomics, the employment of triple sequencing for full-length absolute quantification serves to enhance the precision and reliability of species abundance. The discovery and validation sets were established with the objective of significantly reducing the inherent variation between different human fecal samples. Secondly, previous studies on gut microbiota in IAs patients have zeroed in aneurysm formation, emphasizing the protective role of specific amino acids, such as taurine, in the regulation of amino acid metabolism by the host flora.[7,29] This research presents evidence that gut dysbiosis contributes to the occurrence of rupture events of UIAs. A multi-omics analysis identified multiple core gut flora associated with RIAs, including *Faecalibacterium*, *Roseburia*, *Lachnospira*, and *Blautia*. Furthermore, a suite of amino acids (L-histidine, D-proline, L-methionine, L-lysine, etc.) and FAs (linoleic acid, α-linolenic acid, butyric acid, etc.) were identified as being linked to RIAs. The significance of the FA metabolism and amino acid disorders caused by gut flora imbalance in IA rupture events is underscored by the elucidation of regulatory networks encompassing gut flora and metabolites. The establishment of excellent diagnostic models for differential species and metabolites demonstrates the great potential of gut microbiota as a predictive factor for the risk of aneurysm rupture. Interestingly, our findings for different sites of IAs demonstrated a close association between intestinal flora and the sites with a high rupture risk for IAs. Furthermore, some species dysbiosis (*Roseburia*, *Agathobacter*, *Butyricicoccus*, *Blautia*, etc.) were not only involved in the rupture event of aneurysms but also closely associated with the site of aneurysm occurrence. This has not been previously mentioned in previous studies. Finally, the identification of PB and intraoperative CSF samples confirmed that FAs and amino acid imbalance is mediated by the MGBA and participates in the rupture process of IAs through the BBB (Figure 7).

The composition of the gut flora is vulnerable to factors such as age, gender, and particularly diet.[17,31] For the selection of participants in the healthy control group, we purposively chose relatives of similar age who cohabited and shared meals with the patients diagnosed with UIAs. Concurrently, we established two cohorts, the discovery set, designed for initial exploration and hypothesis generation, and the validation set, intended for confirmatory analysis and validation of findings. This approach aimed to minimize the impact of potential confounding factors unrelated to the aneurysm on species composition and thereby enhance the rigor of sample analysis. Distinct from prior investigations on gut flora in patients with IAs, our study employed full-length absolute quantification, leveraging triple-sequencing technology.[32] Results not only are more precise but also possess superior species resolution compared to second-generation sequencing and V3-V4 variable region detection methods. The etiology of IA rupture is now widely believed to be intricately linked to inflammation of the vascular endothelium and the transformation of vascular smooth muscle cells into a secretory phenotype.[33,34] The imbalance in gut microbiota is widely recognized as leading to a decrease in beneficial bacteria and a concomitant increase in harmful microbes. Both the discovery and validation cohorts of microbiomics data revealed a notable decrease in diverse gut probiotics, including *Blautia* and *Roseburia*. These species are all significant contributors to the production of butyric acid, an SCFA that exhibits potent anti-inflammatory properties through intracellular HDAC inhibition and suppression of nuclear factor κB activation.[35,36] Thus, inflammation of the arterial vascular wall within the cranium, attributed to intestinal dysbiosis, may serve as a pivotal factor in the rupture of aneurysms.

Previous metabolomics studies have primarily focused on the PB of patients with IAs, with limited attention paid to fecal metabolomic analysis.[37] Through a combined analysis of gut microbiota and metabolites, we can better elucidate the role of the MGBA in the development and progression of IAs. Extensive cohort studies conducted in China have revealed significant dysregulation of SCFAs, particularly oleic acid and arachidonic acid, in the PB of patients with high-risk UIAs. These SCFAs potentially serve as protective factors against aneurysm rupture.[38] Our findings not only corroborate the protective role of SCFAs but also reveal dysregulation of linoleic acid and α-linolenic acid in fecal samples from patients with RIAs. These observations are consistent with those reported in PB and CSF samples. Furthermore,

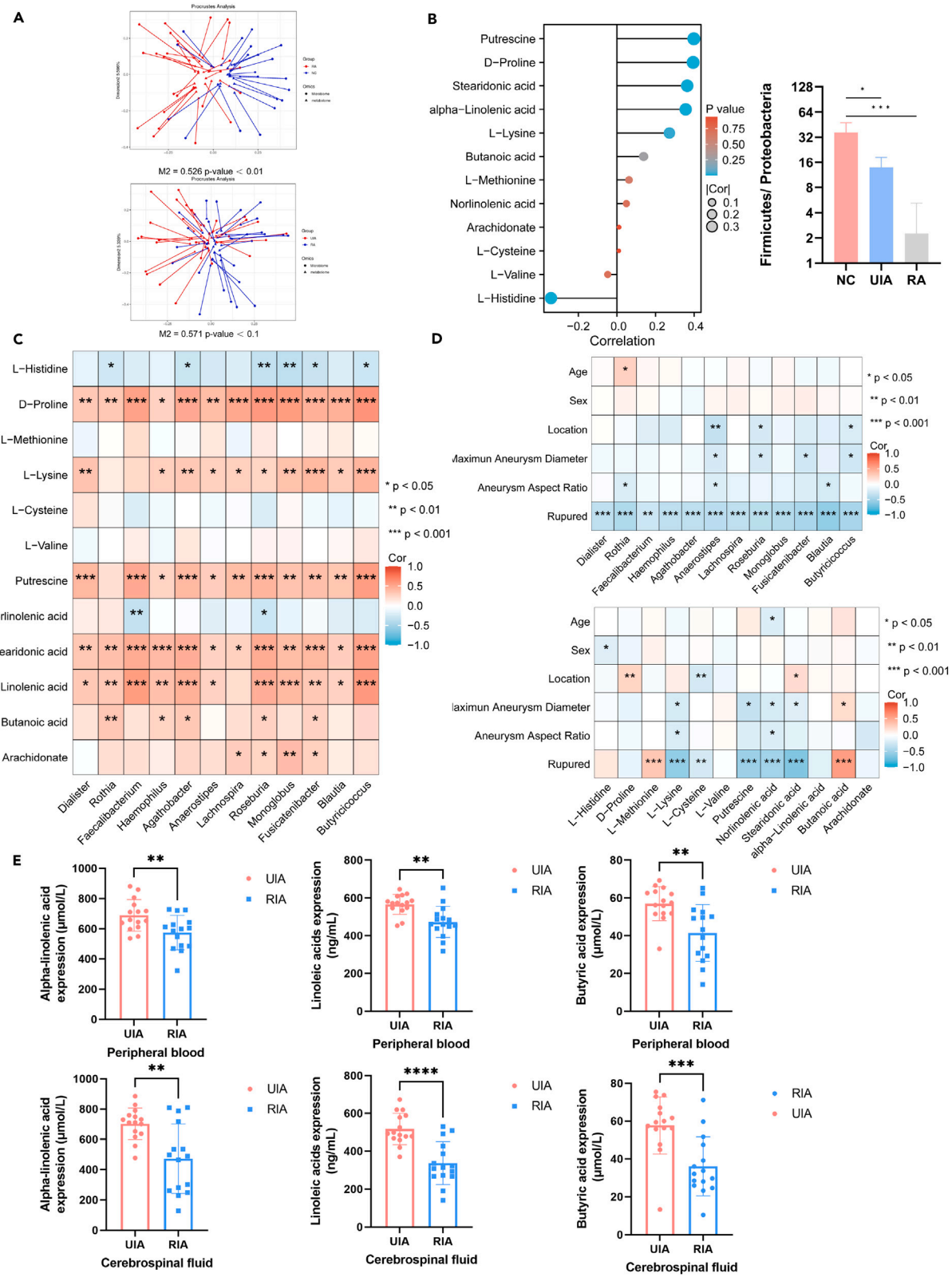
A
M2 = 0.526 p-value < 0.01
M2 = 0.571 p-value < 0.1
B
Putrescine
D−Proline
Stearidonic acid
alpha−Linolenic acid
L−Lysine
Butanoic acid
L−Methionine
Norlinolenic acid
Arachidonate
L−Cysteine
L−Valine
L−Histidine
P value
0.75
0.50
0.25
|Cor|
0.1
0.2
0.3
Correlation
Firmicutes/ Proteobacteria
NC
UIA
RA
C
D
* p < 0.05
** p < 0.01
*** p < 0.001
Cor
Dialister
Rothia
Faecalibacterium
Haemophilus
Agathobacter
Anaerostipes
Lachnospira
Roseburia
Monoglobus
Fusicatenibacter
Blautia
Butyricicoccus
Age
Sex
Location
Aneurysm Aspect Ratio
Rupured
E
Alpha-linolenic acid expression (μmol/L)
Linoleic acids expression (ng/mL)
Butyric acid expression (μmol/L)
UIA
RIA
Peripheral blood
Cerebrospinal fluid

Figure 5. Combined multi-omics analysis of the gut microbiome and its metabolites in IA patients

(A) Concordance of microbiome and metabolomics data compared by Procrustes analysis.

(B) Alterations in the F/P ratio among IAs and correlation with differential metabolites (one-way ANOVA, mean with SD). *p* value, $*p < 0.05$; $***p < 0.001$.

(C) Correlation analysis between differential flora and metabolites (Pearson correlation). *p* value, $*p < 0.05$; $**p < 0.01$; $***p < 0.001$.

(D) Multi-omics combined with comprehensive analysis of clinical information and aneurysm characteristics. (Pearson correlation). *p* value, $*p < 0.05$; $**p < 0.01$; $***p < 0.001$.

(E) Determination of α-linolenic, linoleic, and butyric acids in CSF and PB samples (Student's t test, mean with SD). *p* value, $**p < 0.01$; $***p < 0.001$; $****p < 0.001$.

the diagnostic model constructed using the differential gut microbiota and metabolites identified in the discovery set samples exhibited excellent predictive performance, which was thoroughly validated in the validation set. Our future research will focus on exploring whether the supplementation of linoleic acid, α-linolenic acid, and essential amino acids can reduce the occurrence of aneurysm rupture. Furthermore, an investigation into whether an increased intake of SCFAs can improve the prognosis and reduce the occurrence of neurological sequelae in RIA patients is warranted.

In summary, the research described the dysregulation of gut microbiota and metabolites in IA patients, particularly RIAs, and identified key differential species and metabolites. A strong correlation between dysregulation of SCFAs and essential amino acid metabolic pathways with risk factors for rupture of IAs has been proposed. PB and CSF sample validations have further confirmed the pivotal roles of linoleic acid, α-linolenic acid, and butyric acid. Integrating clinical features, we have further uncovered alterations in the gut microbiota of patients with high-risk aneurysm rupture locations. The construction of a robust diagnostic model suggests that gut microbiota and metabolite biomarkers have the potential to predict the risk of aneurysm rupture.

Limitations of the study

Admittedly, this study also has some limitations. Our research population was limited to middle-aged and elderly individuals from central China. Compared to multi-center studies, further validation with a larger sample size is needed in the future. Due to the complexity of IA model construction, the *in vivo* validation of the identified differential microbiota and metabolites remains a crucial aspect of our future research that requires further exploration.

RESOURCE AVAILABILITY

Lead contact

Further information and requests for the data should be directed to and will be fulfilled by the lead contact, Xiang Li (li.xiang@whu.edu.cn).

Materials availability

This study did not generate reagents.

Data and code availability

- The raw 16S rDNA gene sequencing data in this study have been deposited in the Genome Sequence Archive (GSA) and are publicly available as of the date of publication (HRA007513). Accession numbers are listed in the key resources table.
- The metabolomics data reported in this paper have been deposited in the OMIX, China National Center for Bioinformation/Beijing Institute of Genomics, Chinese Academy of Sciences, and are publicly accessible (OMIX007574).
- This paper does not report original code.
- Any additional information required to reanalyze the data reported in this paper is available from the lead contact upon request.

ACKNOWLEDGMENTS

This work was supported by the National Natural Science Foundation of China (82001421) and the Climbing Project for Medical Talent of Zhongnan Hospital, Wuhan University. We acknowledge the contributions of our laboratory colleagues in the preparation of this article.

AUTHOR CONTRIBUTIONS

H.X. performed the experiments and wrote the manuscript; H.X., Z.L., and S.L. participated in analysis and drafted the manuscript; H.X., Q.Z., X.L., G.L., and Z.X. collected the clinical samples; W.W. and J.C. edited and revised the manuscript; X.L., W.W., and Z.L. designed and funded the project. All authors approved the manuscript for publication.

DECLARATION OF INTERESTS

The authors declare no competing interests.

STAR★METHODS

Detailed methods are provided in the online version of this paper and include the following:

- KEY RESOURCES TABLE
- EXPERIMENTAL MODEL AND SUBJECT DETAILS
  - Recruitment of study participants

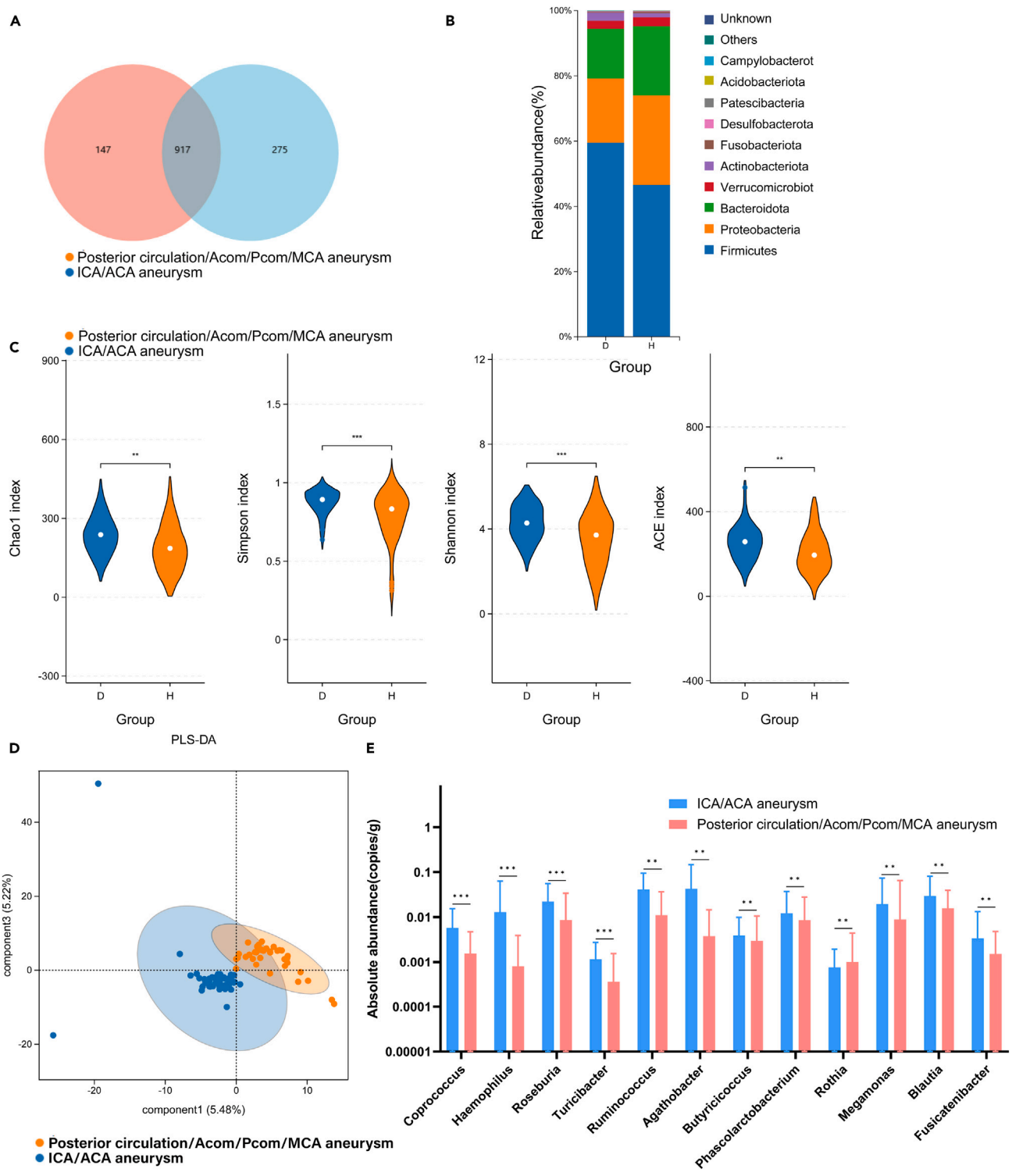

Figure 6. Altered gut microbiome in patients with IAs is tightly linked to site of occurrence

(A) Venn diagram depicting the quantity of both shared and distinct OTUs among various groups.

(B) Species composition of the gut microbiota in groups at the portal level.

(C and D) Alpha diversity index variance analysis and beta diversity analysis in the high-rupture-risk group (Wilcoxon test, mean with SD). *p* value, $^{**}p < 0.01$; $^{***}p < 0.001$.

(E) Identification of gut microbiota associated with locations at high risk of rupture (t test, mean with SEM). *p* value, $^{**}p < 0.01$; $^{***}p < 0.001$.

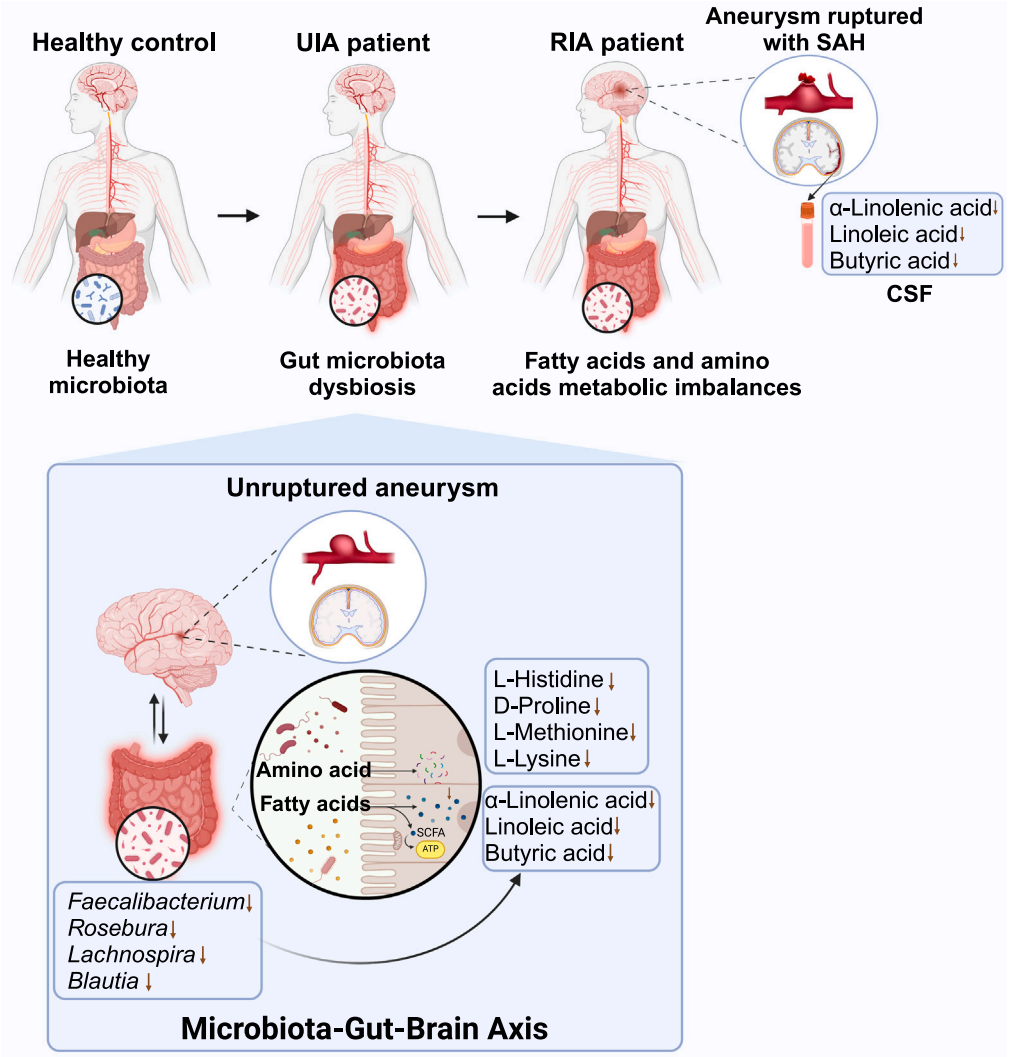

Figure 7. Dysregulation of SCFA and amino acid metabolism induced by gut disorders mediates IA rupture events via the MGBA

SUPPLEMENTAL INFORMATION

Supplemental information can be found online at https://doi.org/10.1016/j.isci.2024.111184.

Received: May 18, 2024
Revised: August 27, 2024
Accepted: September 30, 2024
Published: October 16, 2024

REFERENCES

1. Xiong, Y., Zheng, Y., Yan, Y., Yao, J., Liu, H., Shen, F., Kong, S., Yang, S., Yan, G., Zhao, H., et al. (2022). Circulating proteomic panels for risk stratification of intracranial aneurysm and its rupture. EMBO Mol. Med. *14*, e14713. https://doi.org/10.15252/emmm.202114713.
2. Claassen, J., and Park, S. (2022). Spontaneous subarachnoid haemorrhage. Lancet *400*, 846–862. https://doi.org/10.1016/s0140-6736(22)00938-2.
3. Chen, Y., Wright, N., Guo, Y., Turnbull, I., Kartsonaki, C., Yang, L., Bian, Z., Pei, P., Pan, D., Zhang, Y., et al. (2020). Mortality and recurrent vascular events after first incident stroke: a 9-year community-based study of 0·5 million Chinese adults. Lancet Global Health *8*, e580–e590. https://doi.org/10.1016/s2214-109x(20)30069-3.
4. Greving, J.P., Wermer, M.J.H., Brown, R.D., Jr., Morita, A., Juvela, S., Yonekura, M., Ishibashi, T., Torner, J.C., Nakayama, T., Rinkel, G.J.E., and Algra, A. (2014). Development of the PHASES score for prediction of risk of rupture of intracranial aneurysms: a pooled analysis of six prospective cohort studies. Lancet Neurol. *13*, 59–66. https://doi.org/10.1016/s1474-4422(13)70263-1.
5. Backes, D., Rinkel, G.J.E., Greving, J.P., Velthuis, B.K., Murayama, Y., Takao, H., Ishibashi, T., Igase, M., terBrugge, K.G., Agid, R., et al. (2017). ELAPSS score for prediction of risk of growth of unruptured intracranial aneurysms. Neurology *88*, 1600–1606. https://doi.org/10.1212/wnl.0000000000003865.
6. Socała, K., Doboszewska, U., Szopa, A., Serefko, A., Włodarczyk, M., Zielińska, A., Poleszak, E., Fichna, J., and Wlaź, P. (2021). The role of microbiota-gut-brain axis in neuropsychiatric and neurological disorders. Pharmacol. Res. *172*, 105840. https://doi.org/10.1016/j.phrs.2021.105840.
7. Morais, L.H., Schreiber, H.L., 4th, and Mazmanian, S.K. (2021). The gut microbiota-brain axis in behaviour and brain disorders. Nat. Rev. Microbiol. *19*, 241–255. https://doi.org/10.1038/s41579-020-00460-0.
8. Qi, X., Yun, C., Pang, Y., and Qiao, J. (2021). The impact of the gut microbiota on the reproductive and metabolic endocrine system. Gut Microb. *13*, 1–21. https://doi.org/10.1080/19490976.2021.1894070.
9. Wang, Q., Yang, Q., and Liu, X. (2023). The microbiota-gut-brain axis and neurodevelopmental disorders. Protein Cell *14*, 762–775. https://doi.org/10.1093/procel/pwad026.
10. Xu, H., Xu, Z., Long, S., Li, Z., Jiang, J., Zhou, Q., Huang, X., Wu, X., Wei, W., and Li, X. (2023). The role of the gut microbiome and its metabolites in cerebrovascular diseases. Front. Microbiol. *14*, 1097148. https://doi.org/10.3389/fmicb.2023.1097148.
11. Peh, A., O'Donnell, J.A., Broughton, B.R.S., and Marques, F.Z. (2022). Gut Microbiota and Their Metabolites in Stroke: A Double-Edged Sword. Stroke *53*, 1788–1801. https://doi.org/10.1161/strokeaha.121.036800.
12. Sampson, T.R., Debelius, J.W., Thron, T., Janssen, S., Shastri, G.G., Ilhan, Z.E., Challis, C., Schretter, C.E., Rocha, S., Gradinaru, V., et al. (2016). Gut Microbiota Regulate Motor Deficits and Neuroinflammation in a Model of Parkinson's Disease. Cell *167*, 1469–1480.e12. https://doi.org/10.1016/j.cell.2016.11.018.
13. Jakaria, M., Azam, S., Haque, M.E., Jo, S.H., Uddin, M.S., Kim, I.S., and Choi, D.K. (2019). Taurine and its analogs in neurological disorders: Focus on therapeutic potential and molecular mechanisms. Redox Biol. *24*, 101223. https://doi.org/10.1016/j.redox.2019.101223.
14. Bogie, J.F.J., Haidar, M., Kooij, G., and Hendriks, J.J.A. (2020). Fatty acid metabolism in the progression and resolution of CNS disorders. Adv. Drug Deliv. Rev. *159*, 198–213. https://doi.org/10.1016/j.addr.2020.01.004.
15. Chidambaram, S.B., Rathipriya, A.G., Mahalakshmi, A.M., Sharma, S., Hediyal, T.A., Ray, B., Sunanda, T., Rungratanawanich, W., Kashyap, R.S., Qoronfleh, M.W., et al. (2022). The Influence of Gut Dysbiosis in the Pathogenesis and Management of Ischemic Stroke. Cells *11*, 1239. https://doi.org/10.3390/cells11071239.
16. Agus, A., Clément, K., and Sokol, H. (2021). Gut microbiota-derived metabolites as central regulators in metabolic disorders. Gut *70*, 1174–1182. https://doi.org/10.1136/gutjnl-2020-323071.
17. Li, H., Xu, H., Li, Y., Jiang, Y., Hu, Y., Liu, T., Tian, X., Zhao, X., Zhu, Y., Wang, S., et al. (2020). Alterations of gut microbiota contribute to the progression of unruptured intracranial aneurysms. Nat. Commun. *11*, 3218. https://doi.org/10.1038/s41467-020-16990-3.
18. Winand, R., Bogaerts, B., Hoffman, S., Lefevre, L., Delvoye, M., Braekel, J.V., Fu, Q., Roosens, N.H., Keersmaecker, S.C.D., and Vanneste, K. (2019). Targeting the 16s rrna gene for bacterial identification in complex mixed samples: Comparative evaluation of second (illumina) and third (oxford nanopore technologies) generation sequencing technologies. Int. J. Mol. Sci. *21*, 298. https://doi.org/10.3390/ijms21010298.
19. Edgar, R.C. (2013). UPARSE: highly accurate OTU sequences from microbial amplicon reads. Nat. Methods *10*, 996–998. https://doi.org/10.1038/nmeth.2604.
20. Osawa, M., Handa, O., Fukushima, S., Matsumoto, H., Umegaki, E., Inoue, R., Naito, Y., and Shiotani, A. (2023). Reduced abundance of butyric acid-producing bacteria in the ileal mucosa-associated microbiota of ulcerative colitis patients. J. Clin. Biochem. Nutr. *73*, 77–83. https://doi.org/10.3164/jcbn.22-86.
21. Zhou, D., Pan, Q., Xin, F.Z., Zhang, R.N., He, C.X., Chen, G.Y., Liu, C., Chen, Y.W., and Fan, J.G. (2017). Sodium butyrate attenuates high-fat diet-induced steatohepatitis in mice by improving gut microbiota and gastrointestinal barrier. World J. Gastroenterol. *23*, 60–75. https://doi.org/10.3748/wjg.v23.i1.60.
22. Ruan, G., Chen, M., Chen, L., Xu, F., Xiao, Z., Yi, A., Tian, Y., Ping, Y., Lv, L., Cheng, Y., and Wei, Y. (2022). Roseburia intestinalis and Its Metabolite Butyrate Inhibit Colitis and Upregulate TLR5 through the SP3 Signaling Pathway. Nutrients *14*, 3041. https://doi.org/10.3390/nu14153041.
23. Faust, K., and Raes, J. (2012). Microbial interactions: from networks to models. Nat. Rev. Microbiol. *10*, 538–550. https://doi.org/10.1038/nrmicro2832.
24. Nilholm, C., Manoharan, L., Roth, B., D'Amato, M., and Ohlsson, B. (2022). A starch- and sucrose-reduced dietary intervention in irritable bowel syndrome patients produced a shift in gut microbiota composition along with changes in phylum, genus, and amplicon sequence variant abundances, without affecting the micro-RNA levels. United European Gastroenterol. J. *10*, 363–375. https://doi.org/10.1002/ueg2.12227.
25. Etminan, N., Brown, R.D., Jr., Beseoglu, K., Juvela, S., Raymond, J., Morita, A., Torner, J.C., Derdeyn, C.P., Raabe, A., Mocco, J., et al. (2015). The unruptured intracranial aneurysm treatment score: a multidisciplinary consensus. Neurology *85*, 881–889. https://doi.org/10.1212/wnl.0000000000001891.
26. Brown, R.D., Jr., and Broderick, J.P. (2014). Unruptured intracranial aneurysms: epidemiology, natural history, management options, and familial screening. Lancet Neurol. *13*, 393–404. https://doi.org/10.1016/s1474-4422(14)70015-8.
27. Gross, B.A., Lai, P.M.R., and Du, R. (2014). Impact of aneurysm location on hemorrhage risk. Clin. Neurol. Neurosurg. *123*, 78–82. https://doi.org/10.1016/j.clineuro.2014.05.014.
28. Qin, H., Yang, F., Hao, P., and Zhang, X. (2023). Gut microbiota and cerebrovascular diseases: a Mendelian randomization study. Front. Microbiol. *14*, 1228815. https://doi.org/10.3389/fmicb.2023.1228815.
29. Ma, C., Zhang, W., Mao, L., Zhang, G., Shen, Y., Chang, H., Xu, X., Jin, H., Li, Z., and Lu, H. (2023). Association of gut microbiome with risk of intracranial aneurysm: a mendelian randomization study. BMC Neurol. *23*, 269. https://doi.org/10.1186/s12883-023-03288-2.
30. Zou, X., Wang, L., Xiao, L., Wang, S., and Zhang, L. (2022). Gut microbes in cerebrovascular diseases: Gut flora imbalance, potential impact mechanisms and promising treatment strategies. Front. Immunol. *13*, 975921. https://doi.org/10.3389/fimmu.2022.975921.
31. Hills, R.D., Jr., Pontefract, B.A., Mishcon, H.R., Black, C.A., Sutton, S.C., and Theberge, C.R. (2019). Gut Microbiome: Profound Implications for Diet and Disease. Nutrients *11*, 1613. https://doi.org/10.3390/nu11071613.
32. Tourlousse, D.M., Yoshiike, S., Ohashi, A., Matsukura, S., Noda, N., and Sekiguchi, Y. (2017). Synthetic spike-in standards for high-throughput 16S rRNA gene amplicon sequencing. Nucleic Acids Res. *45*, e23. https://doi.org/10.1093/nar/gkw984.
33. Frösen, J., Cebral, J., Robertson, A.M., and Aoki, T. (2019). Flow-induced, inflammation-mediated arterial wall remodeling in the formation and progression of intracranial aneurysms. Neurosurg. Focus *47*, E21. https://doi.org/10.3171/2019.5.Focus19234.
34. Starke, R.M., Chalouhi, N., Ding, D., Raper, D.M.S., McKisic, M.S., Owens, G.K., Hasan, D.M., Medel, R., and Dumont, A.S. (2014). Vascular smooth muscle cells in cerebral aneurysm pathogenesis. Transl. Stroke Res. *5*, 338–346. https://doi.org/10.1007/s12975-013-0290-1.
35. Liu, H., Wang, J., He, T., Becker, S., Zhang, G., Li, D., and Ma, X. (2018). Butyrate: A Double-Edged Sword for Health? Adv. Nutr. *9*, 21–29. https://doi.org/10.1093/advances/nmx009.
36. Chen, G., Ran, X., Li, B., Li, Y., He, D., Huang, B., Fu, S., Liu, J., and Wang, W. (2018). Sodium Butyrate Inhibits Inflammation and Maintains Epithelium Barrier Integrity in a TNBS-induced Inflammatory Bowel Disease

Mice Model. EBioMedicine *30*, 317–325. https://doi.org/10.1016/j.ebiom.2018.03.030.

37. Lasica, N., Raicevic, V., Stojanovic, N.M., Djilvesi, D., Horvat, I., Jelaca, B., Pajicic, F., and Vulekovic, P. (2022). Metabolomics as a potential tool for monitoring patients with aneurysmal subarachnoid hemorrhage. Front. Neurol. *13*, 1101524. https://doi.org/10.3389/fneur.2022.1101524.

38. Liu, Q., Li, K., He, H., Miao, Z., Cui, H., Wu, J., Ding, S., Wen, Z., Chen, J., Lu, X., et al. (2023). The markers and risk stratification model of intracranial aneurysm instability in a large Chinese cohort. Sci. Bull. *68*, 1162–1175. https://doi.org/10.1016/j.scib.2023.05.001.

39. Bolger, A.M., Lohse, M., and Usadel, B. (2014). Trimmomatic: a flexible trimmer for Illumina sequence data. Bioinformatics *30*, 2114–2120. https://doi.org/10.1093/bioinformatics/btu170.

40. Kechin, A., Boyarskikh, U., Kel, A., and Filipenko, M. (2017). cutPrimers: A New Tool for Accurate Cutting of Primers from Reads of Targeted Next Generation Sequencing. J. Comput. Biol. *24*, 1138–1143. https://doi.org/10.1089/cmb.2017.0096.

41. Edgar, R.C., Haas, B.J., Clemente, J.C., Quince, C., and Knight, R. (2011). UCHIME improves sensitivity and speed of chimera detection. Bioinformatics *27*, 2194–2200. https://doi.org/10.1093/bioinformatics/btr381.

42. Altschul, S.F., Gish, W., Miller, W., Myers, E.W., and Lipman, D.J. (1990). Basic local alignment search tool. J. Mol. Biol. *215*, 403–410. https://doi.org/10.1016/s0022-2836(05)80360-2.

43. Robin, X., Turck, N., Hainard, A., Tiberti, N., Lisacek, F., Sanchez, J.C., and Müller, M. (2011). pROC: an open-source package for R and S+ to analyze and compare ROC curves. BMC Bioinf. *12*, 77. https://doi.org/10.1186/1471-2105-12-77.

44. Dugan, T.M., Mukhopadhyay, S., Carroll, A., and Downs, S. (2015). Machine Learning Techniques for Prediction of Early Childhood Obesity. Appl. Clin. Inf. *6*, 506–520. https://doi.org/10.4338/aci-2015-03-ra-0036.

STAR★METHODS

KEY RESOURCES TABLE

REAGENT or RESOURCE	SOURCE	IDENTIFIER
Biological samples		
Stool samples from healthy family members	Patients' healthy family members	N/A
Stool samples from patients with intracranial aneurysms	Patients with intracranial aneurysms	N/A
Critical commercial assays		
Human Butyric Acid (BA) ELISA Kit	MEIAO Biotech	MO-P37982R
Human Linoleic Acid (LA) ELISA Kit	MEIAO Biotech	MO-P38041R
Human α-linolenic acid (ALA) ELISA Kit	MEIAO Biotech	MO-P34071R
Tiangen Fecal Sample DNA Extraction Kit	Tiangen Biotech	DP812
SMRTbell™ Template Prep Kit	Pacific Biosciences	100-222-300
DNA/Polymerase Binding Kit	Pacific Biosciences	100-372-700
Deposited data		
Untargeted metabolomics data	This paper	https://ngdc.cncb.ac.cn/omix: accession no. OMIX007574
Microbiomics data	This paper	https://ngdc.cncb.ac.cn/gsa-human: accession no. HRA007513
Software and algorithms		
BMKCloud Platform	Beijing Biomarker Technologies	www.biocloud.net
Trimmomatic	Bolger et al. (2014)[39]	https://github.com/usadellab/Trimmomatic
Cutadapt	Kechin et al. (2017)[40]	https://cutadapt.readthedocs.io/en/stable/
USEARCH	Edgar et al. (2011)[41]	https://drive5.com/usearch/
BLASTN	Altschul et al. (1990)[42]	https://ftp.ncbi.nlm.nih.gov/blast/executables/blast+/
pROC	Robin et al. (2011)[43]	https://github.com/Logentech/pROC

EXPERIMENTAL MODEL AND SUBJECT DETAILS

Recruitment of study participants

In this consecutive and retrospective study, we recruited patients with IAs admitted to the Department of Neurosurgery, Zhongnan Hospital of Wuhan University, from January 2023 to January 2024, and healthy family members as controls. All IAs were examined by cerebral angiography, and characteristics such as aneurysm size, location, shape, height-width ratio, and whether a single or multiple aneurysms were present. To prevent the interference of antibiotics and intestinal microbial agents on the gut microbiome, all stool samples were collected from patients who had not used antibiotics or gastrointestinal microbiome supplements within the previous two months. All patients with IAs, both UIA and RIA, were previously undiagnosed, and all aneurysms were saccular. Patients under the age of 18, those diagnosed with other cerebrovascular diseases (such as dural arteriovenous fistulas, cerebral arterial dissection, moyamoya disease, etc.), or with a confirmed genetic predisposition to intracranial aneurysm formation (such as polycystic kidney disease or Ehlers-Danlos syndrome type 4) were excluded from the study. Similarly, patients who had used antibiotics within the two months prior to admission were also excluded. A total of 124 stool samples from 87 patients with IAs and 37 healthy family controls were used for full-length absolute quantification 16S rRNA sequencing analysis, in addition to 160 stool samples from 112 patients with IAs and 48 healthy family controls for untargeted metabolomics sequencing. Furthermore, we established discovery sets and validation sets in metabolomic and microbiomics analyses to better illustrate the reliability of the results. Tables 1 and 2 list the clinical characteristics of all participants. Finally, PB and intraoperative CSF samples from thirty patients were recollected to measure the concentrations of butyric acid, α-linolenic acid, and linoleic acid by ELISA.

The mean age of the discovery and validation sets of microbiomics participants in this study was 57.4 ± 8.4 years and 58.5 ± 8.2 years, respectively. Additionally, 56% of the participants were female. The mean age of the discovery and control sets of metabolomics participants was 57.6 ± 8.4 years and 57.7 ± 11.0 years, respectively, and 55% of the participants were female. Gender did not affect the findings in this research. This research was screened and endorsed by the Ethics Committee at Zhongnan Hospital of Wuhan University (2024072K). All

participants or legal representatives in this research have signed an informed consent form, with strict adherence to good clinical practice and the Declaration of Helsinki.

METHOD DETAILS

Samples collection and DNA extraction

A 5 mL peripheral blood (PB) sample was obtained from all participants on the day of admission. For stool sample collection, the UIA patients and family controls provided their samples the following morning. For RIA patients, stool samples were collected within 24 h of admission and before the initiation of any antibiotic treatment to minimize the impact of potential alterations to the gut microbiota. Concurrently, fecal samples were obtained while the RIA patients were anesthetized and sedated to prevent aneurysm rupture during the collection process. Fecal specimens were collected using sterile plastic spoons to obtain approximately 2–4 g samples. The samples are then transferred under strictly aseptic conditions into sterile stool sample containers. Additionally, A 2mL CSF sample was safely collected without compromising the surgical outcome. Fresh fecal, PB and CSF samples from all participants were immediately stored in a −20°C refrigerator after obtaining. On the same day, the samples were transferred to the laboratory via ice-box, and have been stored in a −80°C freezer to ensure the quality and accuracy of the samples. In adherence to a standardized protocol, all fecal samples undergo DNA extraction, PCR amplification, library construction, and sequencing in a simultaneous and consecutive manner. These procedures are carried out in strictly controlled, independent, and sterile environments using sterile tools and containers. To mitigate contamination risks from environmental sources or reagents, DNase-free water was employed as a negative control during both DNA extraction and PCR amplification stages, ensuring the absence of amplification products. Using the Tiangen Fecal Sample DNA Extraction Kit (DP812, Tiangen Biotech, Beijing, China), 5 g of each stool was collected separately and used for DNA extraction. The SMRTbell Template Prep Kit (Pacific Biosciences, Menlo Park, USA) was employed to construct DNA libraries using specific primers to amplify diverse regions of the entire 16S rRNA genome (F: 5′- AGRGTTGATYNTGGCTCAG-3′, R: 5′-TASGGHTACCTTGTTASGACTT-3′). The output cDNA library was assessed for sample quality using concentration (Qubit) and size (Agilent 2100) assays. The on-board libraries were pre-sequenced using the PacBio Binding Kit (Pacific Biosciences, Menlo Park, USA) and third-generation 16s rRNA sequencing on a Sequel II sequencer.

Enzyme-linked immunosorbent assay (ELISA)

ELISA kits (MEIAO Biotech, Shanghai, China) were used to detect α-linolenic acid, linoleic acid, and butyric acid in PB and CSF samples. To test the samples, add diluted standards and samples to the pre-coated microtiter plate. Then, add 100ul of horseradish peroxidase (HRP)-labelled detection antibody and incubate at a constant temperature of 37°C for 1 h. Discard the liquid and add the substrate to the plate. Incubate at 37°C for 15 min, avoiding light. Add the termination solution and measure the optical density (OD) value of each well at 450nm. Finally, calculate the concentration of each sample according to the standard curve.

Metabolites extraction and LC-MS/MS analysis

Weigh 50 mg stool sample for metabolite extraction. LC/MS system consist of two main components: the Waters Acquity I-Class PLUS ultra-high performance liquid tandem mass spectrometer and the Waters Xevo G2-XS QTof high resolution mass spectrometer. The chromatographic separation was achieved using a Waters Acquity UPLC HSS T3 column (1.8um, 2.1*100mm). Untargeted metabolomics of fecal samples was conducted via UHPLC-QTOF-MS, employing either an Agilent 1290 UHPLC or an SCIEX 6600, with the mobile phase composed of A: 0.1% formic acid aqueous solution and B: 0.1% formic acid acetonitrile in both positive and negative ion modes. The injection volume was standardized to 1 μL. Two LC-MS/MS analyses were performed, with the high-resolution mass spectrometer collecting primary and secondary mass spectrometry data in MSe mode under the control of MassLynx V4.2 software. Each data acquisition cycle included dual-channel data acquisition for both low and high collision energies, with collision energy settings ranging from 2V to 40V. The ESI ion source parameters were configured as follows: a capillary voltage of 2000V (positive ion mode) or −1500V (negative ion mode), a cone voltage of 30V, an ion source temperature of 150°C, a desolvent gas temperature of 500°C, a backflush gas flow rate of 50L/h, and a desolventizing gas flow rate of 800L/h.

Microbiomics sequencing data analysis

Absolute quantitative sequencing of three generations of microbial diversity is based on the PacBio sequencing platform and employs single molecule real-time sequencing to sequence marker genes. The BMKCloud Platform (www.biocloud.net) was used to perform the analyses on the 16S rRNA absolute quantitative sequencing data. The NGS data underwent preprocessing using Trimmomatic (v0.33) based on the quality of individual nucleotides.[39] The primer removal and detection methods were performed using Cutadapt (v1.9.1).[40] The PE reads from the preceding steps were assembled with USEARCH (v10.0), followed by chimera removal with UCHIME (v8.1).[19,41] The final effective data, Effective-CCS (Non spike-in) sequences, were obtained by filtering internal reference sequences by BLASTN v2.9.0+ software.[42] The sequence was clustered using USEARCH (v10.0) with similarity greater than 97% (default). Conservative threshold for operational taxonomic units (OTUs) filtration is 0.005%.

Microbiological diversity analysis

Species richness was evaluated utilizing the Chao1 and Ace indexes, while species diversity at OTU level was assessed by the Shannon and Simpson indexes within the framework of alpha diversity analysis. The rarefaction curve was further verified to reflect the species diversity

within each group. For the beta diversity analysis, Non-MetricMulti-Dimensional Scaling (NMDS) analysis and orthogonal partial least squares-discriminant analysis (OPLS-DA) was performed to contrast the similarities in species diversity across samples.

Significant difference analysis

The Kruskal-Wallis (KW) sum-rank test is initially fitted to identify meaningful diversity with respect to the class of interest. A series of pairwise tests between subclasses employing the (unpaired) Wilcoxon rank-sum test is then performed to determine biological significance. Linear discriminant analysis effect size (LEfSe) employs Linear Discriminant Analysis to estimate the effect size of each feature with differential abundance.

Functional prediction

By matching the species composition details generated from the 16S sequencing data, the PICRUSt software was implemented to predict the functional composition in the samples and to interpret the functional divergence between the groups. BugBase predicts biological level coverage and biologically interpretable phenotypes of functional pathways in complex microbiomes.

Prediction model

The relative abundance of gut flora at the genus level was classified using random forest classification (random Forest v4.6-10 classification algorithm using the R package v3.1.1), which was applied to investigate risk biomarkers to distinguish between UIAs and RIAs.[44] The critical species identified by random forest were analyzed using a multifactorial logistic regression model, followed by Receiver Operating Characteristic (ROC) analysis with the pROC (v1.18.0) package, and the results were visualized using ggplot2 (v3.3.6).[43] Finally, the constructed aneurysm rupture risk prediction model was externally validated through a validation set.

Metabolomics sequencing data analysis

The raw data were acquired by MassLynx V4.2 and normalized to total peak area with QI software from Progenesis for subsequent analysis. Repeatability of the within-group and QC samples was judged by principal component analysis. Annotation of identified metabolites against KEGG, HMDB and lipidmaps databases. Computation and comparison were based on the grouping of normal control group, UIA group as well as RIA group. To assess the significance of the differences, the *p*-value for each group was calculated by T test. Differential metabolites were selected according to a combined approach based on multiplicity of differences, P-value and VIP-value of the OPLS-DA model. The screening criteria were fold change (FC) > 1, p value < 0.05, and VIP>1. Differential metabolites mapping volcanoes by R package (ggplot2). The functions and pathways of selected metabolites were investigated in the KEGG database. In addition, the metabolic pathways were enriched for the individual metabolites.

Multi-omics analysis based on fecal metabolomics and microbiomics data

Procrustes analysis was conducted to measure the consistency of microbiome and metabolomics data by analyzing shape distributions. Spearman correlations between differentially enriched flora and metabolites were computed utilizing the scipy-stats software package (v0.14.1) in python (v2.7.8). The results are presented in heatmaps.

QUANTIFICATION AND STATISTICAL ANALYSIS

Biodiversity and similarity analysis using the OTUs with QIIME2. NMDS analysis is based on the Binary-Jaccard algorithm for dimensionality reduction analysis, which displays the same groups of samples as 95% confidence ellipses. PCA analysis of metabolomics samples by calculating the covariance matrix. Gut microbiota from multiple groups were compared at the genus level by enrichment analysis of differences using the Kruskal-Wallis rank-sum test and corrected for *p*-values using the BH-FDR method. Metastats analysis was performed to t-test species abundance between the two groups to obtain *p*-values and corrected q-values to screen for differing species. PLS-DA was utilized to differentiate metabolites between the two groups and obtain VIP values while screening for differential metabolites in combination with *p*-value and fold change. Procrustes analysis selected PCoA to down-rank the species (at the genus level) and metabolisms, respectively, and calculated distance matrices using the microbial quantification matrix and the metabolite quantification matrix. The distance algorithm was Bayesian distance for microbes and Euclidean distance for metabolome. For both PB and CSF ELISA, two-tailed unpaired Student's t-test was used to analyze differences between the UIA and RIA patients. Statistical significance was determined as $p < 0.05$, $*p < 0.05$; $**p < 0.01$; $***p < 0.001$; $****p < 0.001$.